Arabian Journal of Chemistry (2022) **15**, 104120

King Saud University

Arabian Journal of Chemistry

www.ksu.edu.sa
www.sciencedirect.com

ORIGINAL ARTICLE

The superior adsorption capacity of phenol from aqueous solution using Modified Date Palm Nanomaterials: A performance and kinetic study

Fahad M. Alminderej [a,*], Alaa M. Younis [a,b], Abuzar E.A.E. Albadri [a], Wael A. El-Sayed [a,c], Yassine El-Ghoul [a,d], Reham Ali [a,e], Adel M.A. Mohamed [f], Sayed M. Saleh [a,g,*]

[a] *Department of Chemistry, College of Science, Qassim University, Buraidah 51452, Saudi Arabia*
[b] *Aquatic Environment Department, Faculty of Fish Resources, Suez University, Suez 43518, Egypt*
[c] *Photochemistry Department, National Research Centre, Dokki, Giza, Egypt*
[d] *Textile Engineering Laboratory, University of Monastir, Monastir 5019, Tunisia*
[e] *Chemistry Department, Science College, Suez University, 43518 Suez, Egypt*
[f] *Department of Metallurgical and Materials Engineering, Faculty of Petroleum and Mining Engineering, Suez University, Suez 43512, Egypt*
[g] *Chemistry Branch, Department of Science and Mathematics, Faculty of Petroleum and Mining Engineering, Suez University, 43721 Suez, Egypt*

Received 5 June 2022; accepted 8 July 2022
Available online 16 July 2022

KEYWORDS

Adsorption;
Pollutant;
Date palm;
Adsorption capacities;
Phenol

Abstract This work investigates the prospective usage of dried Date palm fibers (DPF) and amino silica modified Date palm fibers nanomaterials (Si-DPF) for phenol removal from water. We studied the characteristics of both dried DPF and Si-DPF nanomaterials based on their composition and morphology. The characterization includes diverse types of instruments such as Fourier-transform infrared spectroscopy (FTIR), Brunauer Emmett Teller (BET), scanning electron microscopy (SEM), and transmission electron microscope (TEM). Batch mode experimentations were continued and studied utilizing various significant factors such as the dose of adsorbent, solution pH, contact time, and the initial quantity of phenol molecules as a pollutant. Under optimum conditions (pH: 7.00, adsorbent dose: 2.00 g/L, initial concentration of phenol: 100 ppm and contact time: 24 h), the maximum adsorption capacities were calculated to be 19.57 and 31.25 mg/g for DPF and Si-DPF respectively. Further, to study the mechanism of the adsorption process of the

* Corresponding authors.
E-mail addresses: F.alminderej@qu.edu.sa (F.M. Alminderej), e.saleh@qu.edu.sa (S.M. Saleh).
Peer review under responsibility of King Saud University.

Production and hosting by Elsevier

https://doi.org/10.1016/j.arabjc.2022.104120

under-investigated toxic molecules on the active sites of the nanomaterials, we introduced kinetic models involving pseudo-first-order, pseudo-second-order, and models based on intra-particle diffusion. To study the equilibrium isotherms, the Langmuir and Freundlich isotherms were considered, and the Langmuir isothermal model ($R^2 \approx 0.997$ and 0.984 for DPF and Si-DPF respectively) which largely deals with the results of the experiments achieved.

1. Introduction

Date palm fibers (DPF) are one of the waste materials of the date palm (Phoenix dactylifera L.) tree. DPF can grow any over the world but will produce fruits in different countries (Ahmad et al., 2012; Alotaibi et al., 2019; Ghori et al., 2018; Saker et al. 2006); in general, date palm fibers waste is estimated at 20 kg per tree (AL-Oqla et al., 2014; Alshabanat et al., 2016). Pharaohs and the Romans used PDF in various industries until recent times, such as ropes, baskets, pillows, and cleaning equipment (Elbadry 2014). Date palm fibers consist of four kinds of fiber: leaf fiber in the peduncle, baste fiber in the stem, wood fiber in the trunk, and surface fiber around the trunk (Hassan and Salih 2016). They mainly consist of the palm fiber are holocellulose 60–75 % embedded in phenylpropane polymer units. Considerable C—O—C or C—C bonds called lignin, bind the main fiber structure and act as cementing material (20 %) and ash (1.18 %) (Alotaibi et al., 2019; Ghori et al., 2018).

Several methods are available with a fluctuating level of success to remove the phenol and other chemical pollutants from water and wastewater (Azari et al., 2015; Berizi et al., 2016; Moghaddam et al., 2019). These developed methods include chemical, physical, and biological treatments. The chemical methods include reduction, oxidation, precipitation, solvent extraction, ion exchange, electrolysis, and photochemical reactions (Azari et al., 2021; Badi et al., 2019; Esrafili et al., 2016). Additionally, physical treatments were presented, such as filtration membrane separation, reverse osmosis, coagulation, flocculation, evaporation, irradiation by nuclear radiations, ultrasonic, magnetic separation, and adsorption (Eryılmaz and Genc, 2021; Guo et al., 2022; Sanchez et al., 2018; Yousefzadeh et al., 2017). And biological treatment involves the aerobic and anaerobic treatment, microbial reduction, and bacterial treatment (Gül et al., 2019; Guo, et al., 2018; Mani and Hameed, 2019). All these methods have extreme expenses, creating toxic components and energy consumption compared to adsorption methods in the case of adsorbent materials supplied from agricultural wastes. Therefore, agriculture waste adsorbents are becoming the aim of many types of research. These involve agro-waste of sugarcane, olive, bagasse, bamboo, soy, mango, orange, coconut, pumpkin, palm, cotton, and rice (Moreno-Marenco et al., 2020; Ahmad, and Alrozi 2011; Lalhruaitluanga et al., 2010; Dahiya and Nigam 2020; Routoula and Patwardhan 2020). Because of the steady increase in the cost of adsorbent materials, no one can deny that a cost-effectively practical solution to this challenge ought to involve the development of environmentally friendly waste materials into valuable materials for adsorption process application.

Scientists examined various agricultural wastes as biosorbents for phenol removal. Various scientific research has reported that date palm has been of tremendous significance as activated carbon of different date palm parts were examined as biosorbents for phenol removal (Pasalari et al., 2017; Saleem et al., 2019; Khurshid et al, 2022). Besides, DPF was used as a biosorbent for specific types of hazardous dyes from an aqueous solution (Alshabanat et al., 2013). However, there is no information on removing phenolic compounds from water using DPF in the literature, particularly on the surface fibers around the trunk. In addition, this research selected DPF as a novel biosorbent due to its biological features like availability in abundance at fibrous form, biodegradability, sustainability, lower pollutant emissions, lower cost, and feasibility for deriving, have a rough and uneven surface, renewable (Hassan and Salih 2016; Ahmad et al., 2012).

Several utilized nanomaterials were used as solid-phase adsorbent particles. Silica nanomaterials show valuable characteristics involving decisive adsorption efficacies due to their chemical properties (Saleh et al., 2010; Ali et al., 2016), active and immense surface area (Mader et al., 2008; Youssif et al., 2018a, 2018b), considerable adsorbability with the noteworthy spreading of regular pore size (Youssif et al., 2018a, 2018b; Wang et al.,2015). Furthermore, their distinctive properties include high dispersion in aqueous solution, precious mechanical and thermal stability, and introducing an excessive stability range under a wide range of temperatures (Thommes et al., 2015; Saleh et al., 2011). Moreover, their particle modification diversity is an extra important feature. Thus, several industrial applications were developed involving adapted fluid silica nanomaterials or microparticles employing the batch method (Du et al., 2014; Karim et al., 2012). The silica nanomaterials are safe and efficiently cost-effective materials presenting a tremendously broad range of surface alteration because of active silanol. Indeed, the silanol groups that present in the silica linker structure give the material the ability for labeling different inorganic or natural materials. The modification process to produce silica-coated nanomaterials is an extreme significant feature. These forms include mesoporous, amorphous gels, and fumed silica particles (Singh et al., 2014; Sun et al., 2015).

We have designed and produced for new materials of dispersed Si-DPF nanomaterials using a synthesis technique depending on the Stöber method (Stöber 1968; Saleh et al., 2019). The purpose of this technique is to increase the material adsorption characteristic. The prepared Si-DPF nanomaterials offer better adsorption ability and excellent water dispersion effectiveness concerning plain DPF. Therefore, the current research investigates the potential of DPF and Si-DPF nanomaterials for water treatment from dangerous pollutants involving toxic phenol removal for the first time. The influence of diverse factors, for instance, adsorbent concentration, phenol molecule content, and contact time, on the adsorption efficiency, were correspondingly investigated. Lastly, the proper conditions of the experiment series, kinetics, and the isotherm (Langmuir and Freundlich) equations were investigated.

2. Materials and methods

2.1. Materials

Tetraethyl orthosilicate (TEOS) 98 %, (3-Aminopropyl) trimethoxysilane (APTS) 97 %, phenol, and ammonia solution 28 % were all used as obtained from the Sigma Aldrich Company. DPF is provided as waste materials in agriculture sector, Qassim region, Saudi Arabia. The stock standard solutions of 1 g/L of phenol were prepared in bi-distilled water and kept in a dark glass container at −4 °C. The different phenol concentrations were prepared by diluting from stock solutions using bi-distilled water at once before use in each experiment.

0.45 μm membrane filter paper (GF/C Whatman) was used to filter the samples before analysis. Vis/UV Spectrophotometer-19 (SCO-Tech, Germany) was used for absorbance measurements.

2.2. Preparation of DPF

DPF materials were collected from the Qassim region, washed using stream water then using distilled water. After washing the obtained DPF materials were dried at room temperature and mechanically ground in an agate mortar. The DPF materials were sieved in analytical sieves to exclude the big particles. Lastly, the resulting fine powder was conveyed to a planetary ball mill to be ground into nano-particles before use.

2.3. Preparation of Si-DPF nanomaterials

The Si-DPF nanomaterials were prepared according to (Stöber et al.,1968). Typically, 150 mg of the DPF nanomaterials was added into a solution mixture having 100 mL of ethanol, 250 μL bi-distilled water, and 250 μL of ammonia solution at 40 °C for 30 min with vigorously stirring. After that 100 μL, TEOS was added to the obtained solution mixture with slow stirring for 4 h under the same conditions. To introduce the coated DPF nanomaterials surface, 100 μL of APTS was added to the reaction and gently stirred for another 4 h with a 150-rpm rate and exact temperature. The obtained nanomaterials were centrifuged and washed several times with ethanol and acetone and kept for dryness at 60 °C.

2.4. Batch biosorption experiments

The influence of distinct factors on the adsorption efficiency was investigated using batch mode techniques. Adsorbent dose, contact time, pH of the solution, and initial concentration were studied to investigate the optimal adsorption efficiency of phenol onto DPF and Si-DPF nanomaterials. In 50-mL stoppered conical flasks, 100 mg of the DPF and Si-DPF nanomaterials were soaked into 50 mL of an aqueous solution with a different concentration of phenol then the mixtures were mechanically shaken at room temperature. Adsorption of phenol using DPF and Si-DPF nanomaterials was performed with different time intervals for sampling at 3, 6, 12, 18, 24, and 36 h while the other factors such as sorbent dosage, pH, and initial concentration of phenol were kept constant. The influence of adsorbent dosage was also investigated by shaking different amounts of DPF and Si-DPF nanomaterials ranging from 10 to 250 mg with a defined amount of aqueous solution containing 100 ppm of phenol for 24 h. To investigate the effect of the initial concentration of phenol, batch sorption tests were performed at different concentrations of phenol 10 to 200 ppm while the other factors including sorbent dosage and contact time kept constant.

The samples were collected from the Erlenmeyer flask at prearranged time intervals and filtrated before analysis. The residual concentrations of phenol were investigated with a colorimetric method using Vis/UV Spectrophotometer. To reduce the errors of the measurement, all the experiments were conducted in triplicate for 24 h at room temperature and the mean values were investigated for further calculations. To find phenol ions loss during the adsorption, negative controls (with no adsorbent) were simultaneously carried out under the same conditions. The amount of adsorbed phenol at equilibrium, q_e (mg/g) into DPF and Si-DPF nanomaterials was computed as the difference between the initial and equilibrium concentrations according to the equation given below.

$$\boldsymbol{q_t = \frac{(C_o - C_t)V}{m_s}}$$

Where.

q_e = amount of adsorbed (mg/g),

C_o = initial concentrations of liquid phase (mg/L).

C_t = the equilibrium concentrations of liquid phase (mg/L).

V = the volume of the solution (L), and X is the mass of DPFNPs and Si-DPF nanomaterials.

The percentage of adsorption (E %) of the DPF and Si-DPF nanomaterials was computed according to the following equation:

$$E\% = \left[\frac{C_o - C_e}{C_o}\right] x100$$

Where:

C_o = initial concentration of phenol (mg/L).

C_e = equilibrium concentration of phenol in aqueous solution (mg/L).

2.5. Adsorption capacity analysis

The adsorption capacities of DPF and Si-DPF nanomaterials were calculated using the following equation.

$$q_t = \frac{(C_o - C_t)V}{m_s}$$

Where:

q = amount of phenol adsorbed by the DPF and Si-DPF nanomaterials (mg/g).

C_o = initial phenol concentrations (mg/L).

C_t = equilibrium phenol concentrations (mg/L).

V = volume of phenol solution (L).

M = mass of biosorbent nanomaterials (g).

2.6. Equilibrium biosorption isotherm models

The equilibrium relationship between pollutants and adsorbents (DPF and Si-DPF) was analyzed using Freundlich and Langmuir isotherm models. This can help to express how the phenol interacts with DPF and Si-DPF nanomaterials and investigate its equilibrium concentrations in the aqueous solution under a constant temperature. The linear form of the Langmuir and Freundlich isotherms is specified by the following equations:

$$\text{Langmuir equation}: \frac{\mathbf{C_e}}{\mathbf{Q_e}} = \frac{1}{\mathbf{Q_{max}K_L}} + \frac{\mathbf{C_e}}{\mathbf{Q_{max}}}$$

$$\text{Freundlich equation}: \mathbf{Log\, Q_e} = \mathbf{log\, K_f} + \frac{1}{\mathbf{n}}\mathbf{Log\, C_e}$$

Where q_e (mg/g) is defined as the mass of phenol adsorbed per mass unit of adsorbent at equilibrium). C_e (mg/L) is the equilibrium concentration of the remaining phenol in an aqueous solution. Q_{max} (mg/g), is the maximum specific uptake cor-

responding to the monolayer saturation. K_L and K_F are Langmuir constant and Freundlich constants, respectively. n is an empirical parameter indicator of adsorption intensity that varies according to the surface heterogeneity of the adsorbent.

3. Results and discussion

3.1. Bio-sorbent nanomaterials characteristics:

3.1.1. FTIR analysis.

FTIR spectra of the DPF and Si-DPF nanomaterials are shown (Fig. 1). The chemical structure of the adsorbent materials includes several chemical groups such as hydroxyl groups of carbohydrate (hemicellulose and cellulose) and lignin (Ragab et al., 2021). Cellulose is the principal component that exists in the DPF. A wideband found at 3310 cm^{-1} distinctive stretching from vibrations of the bonded hydroxyl groups of carbohydrate, this compound presents in DPF include (hemicellulose and cellulose) and lignin (Raghavendra and Lokesh 2019). The 2900 cm^{-1} characteristic band introduces the aliphatic fiber chain. The peak at 1748 cm^{-1} shows the carbonyl group stretching of the carboxylic acid acetyl groups of the lignin compound. The peak at 1620 cm^{-1} refers to C—H, and 1535 cm^{-1} introduces the -C═C vibrations in DPF. But the peaks at 1242 cm^{-1} and 1034 cm^{-1} introduce -C—O—C- and C—H stretching of cellulose and lignin, respectively. Also, the FTIR spectrum of Si-DPF nanomaterials shows a peak at 1560 cm^{-1} revealed to NH_2 groups, which confirms the surface modification of the palm fiber nanomaterials.

3.1.2. Nanomaterials morphology

DPF and Si-DPF nanomaterials were distinguished based on size and morphology using an advanced instrument (SEM); see Fig. 2a. The images exhibit well-defined dimensions that characterize both DPF and Si-DPF nanomaterials, around 60 to 100 nm. Further, the collected TEM instrument of the Si-DPF nanomaterials confirms the presence of a silica shell on the nanomaterials' outer surface as shown in Fig. 2b. A thin silica coat of ~ 15–30 nm has professionally shelled the particles.

Furthermore, the net charge of the unmodified DPF nanomaterials has been exchanged after the modification process by presenting amino groups to the shell surface of nanomaterials. The surface of the unmodified DPF nanomaterials is found to carry a negative net charge because of the presented hydroxyl groups on the surface of the nanomaterial. The considered zeta potential of the unmodified DPF nanomaterials is –32 mV. Memorably, the surface of Si-DPF nanomaterials changes to provide a potential + 15 mV: this results from the amino groups on the outer shell of the Si-DPF nanomaterials. Also, BET measurements were conducted for DPF and Si-DPF nanomaterials using the Micrometrics instrument model ASAP 2010**.** And the measured values were determined to be 175.77 and 177.45 m^2/g correspondingly.

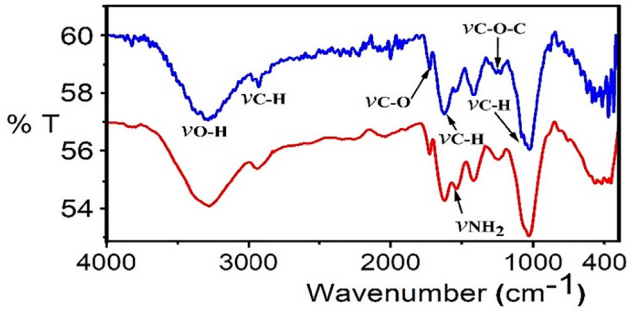

Fig. 1 FTIR data for DPF (blue) and Si-DPF nanomaterials (red).

3.2. Adsorbent dosage influence

The influence of the adsorbent dosage was investigated, which is considered one of the most impact factors on the phenol removal process. This study will supply complete information about the capacity of the adsorbent nanomaterials. The influence of the adsorbent dosage of unmodified DPF nanomaterials on the removal efficacy of phenol from water is shown in Fig. 3. The unmodified DPF nanomaterials dosages were studied within 10 to 250 mg and were exposed to 50 mL, 100 ppm phenol solution. The data exhibits that the adsorption efficiency enhances with the initial concentration increment of the adsorbent nanomaterials. After 100 mg adsorbent dose usage, there is no increment in the removal process. The removal effectiveness percentage of phenol molecules was between 37.5 and 73.85 % for DPF and 47.4 to 82.52 % for Si-DPF nanomaterials. This means that 100 mg of unmodified DPF or modified Si-DPF nanomaterials uptake 73.85 and 82.52 ppm of phenol from an aqueous solution having 100 ppm of phenol concentration.

At the start, the adsorption process of phenol molecules based on un-modified DPF, or modified Si-DPF nanomaterials dosage is directly proportional. The increment of the initial concentration of the adsorbent increases the removal content because of enhancing the surface area and active adoption sites on the adsorbent surface. This will increase the phenol uptake in the first steps up to 100 mg of unmodified DPF or modified Si-DPF nanomaterials. After 100 mg of unmodified DPF or modified Si-DPF nanomaterials adsorbent dose, the adsorption capacities become constant, and the process is almost stable (Siva Kumar and Min 2011). Finally, we can conclude that the optimum concentration of unmodified DPF or modified Si-DPF nanomaterials in the proposed project is 2 g/L.

3.3. Contact time influence

The influence of the shaking time is one of the most impacting factors after the adsorbent dosage to detect the adsorption equilibrium time of the phenol removal process (Dehmani, 2020). The shaking time affects the active surfaces of unmodified DPF or modified Si-DPF nanomaterials based on their accessible active sits of the adsorbents. The influence of contact time on removing phenol proficiency from water is displayed in Fig. 4. The impact of the shaking time on the phenol adsorption processes using DPF and Si-DPF nanomaterials was investigated by varying the contact time from 3 to 36 h. The conditions were adjusted to be 100 mg adsorbent dosage, 100 ppm of phenol molecules content at room temperature, neutral medium, and 200 rpm shaking rapidity. The data shows the maximum removal proficiencies of phenol molecules by unmodified DPF and modified Si-DPF nanomaterials were

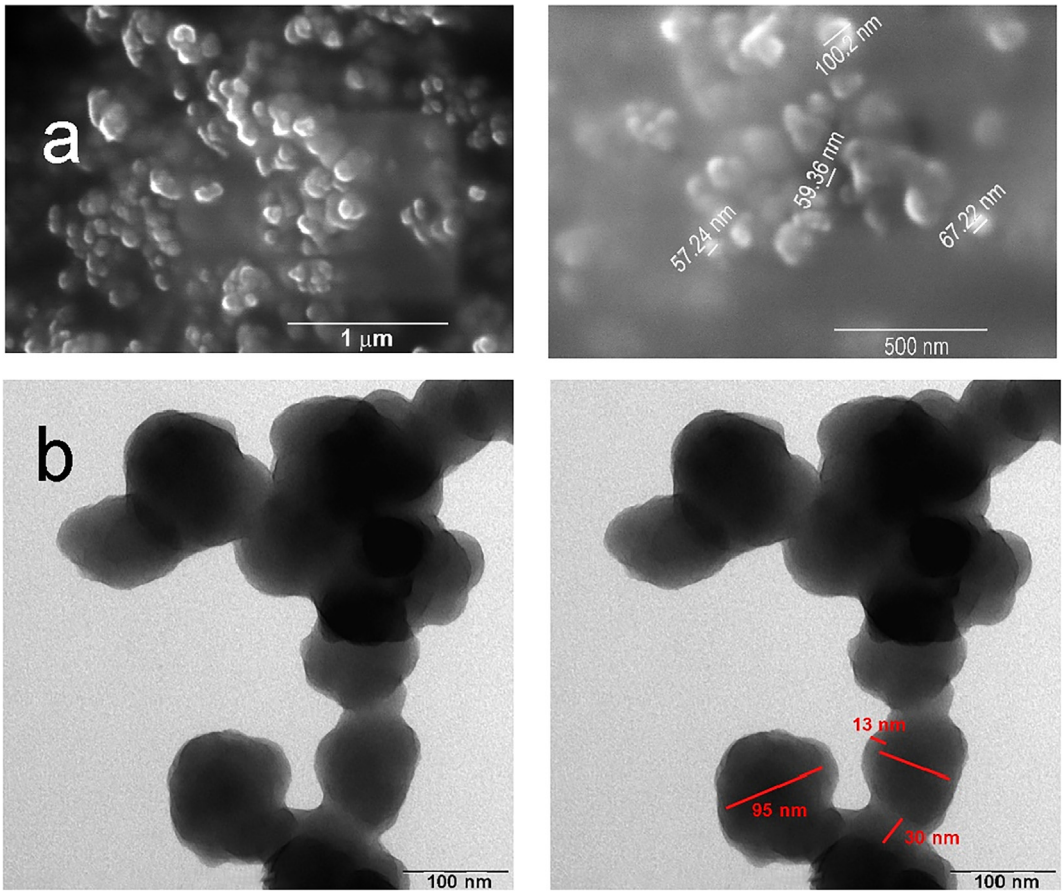

Fig. 2 SEM images for the synthesized nanomaterials (a) DFP nanomaterials; and (b) TEM images of Si-DPF nanomaterials.

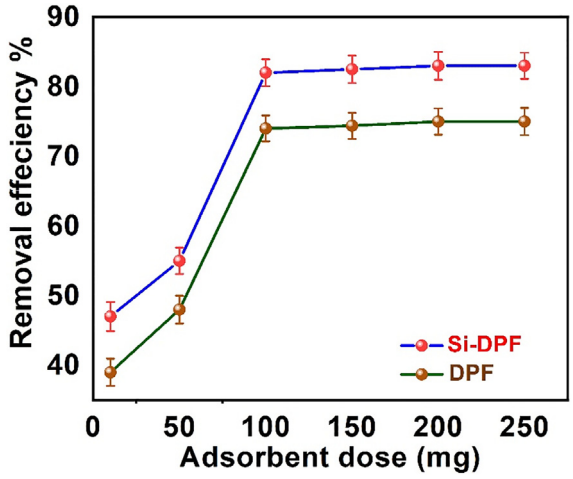

Fig. 3 Influence of DPF (bottom) and Si-DPF (top) nanomaterials contents on the phenol removal processes, [Phenol] = 100 ppm, Reaction time = 24 h, room temperature and neutral pH medium.

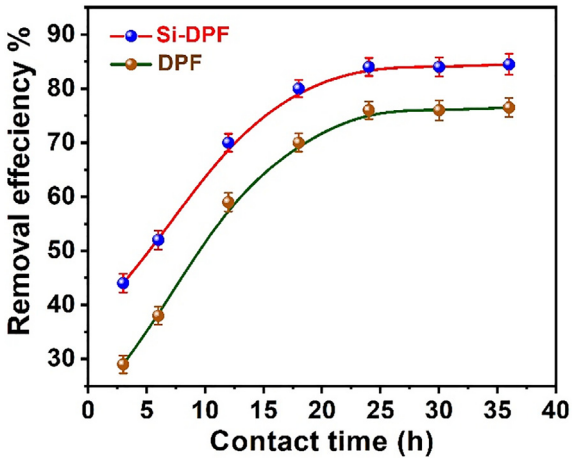

Fig. 4 Contact time efficiency of phenol removal by DPF (bottom) and Si-DPF (top) nanomaterials: [Phenol] = 100 mg/L, reaction time = 24 h, room temperature,and neutral pH medium.

76 and 85 ppm from an aqueous solution containing 100 ppm of phenol concentration. The percentage of adsorption efficiency varied from 29 to 76 % for unmodified DPF and from 43 to 85 % for modified Si-DPF nanomaterials. During the first stage of the absorption process, the adsorption proficiency of the adsorption process on DPF and Si-DPF nanomaterials increases gradually, providing that there are a lot of willingly available functioning sites. Ultimately, flat terrain is attained in the plot representing that the adsorbent is filled.

One can see that the adsorption process's proficiency based on the DPF and Si-DPF nanomaterials attained equilibrium at

24 h. With shielding the active sites of the adsorbent, no noticeable efficiency was noticed after more contact time duration. At equilibrium, the phenol uptake reaches a constant concentration significantly and does not change with time (Younis et al., 2016). Thus, the shaking time was selected to be 24 h, and it is a prosperous time to reach the equilibrium state for the removal process of phenol from the water medium by DPF and Si-DPF nanomaterials.

3.4. Influence of initial phenol concentration

The influence of initial phenol concentration, which alters within (10–200) ppm, on the phenol removal processes based on the bio-sorbent nanomaterials was investigated in a neutral medium and at room temperature. The removal efficiency was studied based on definite concentrations of (10–200 mg/mL) of DPF or modified Si-DPF nanomaterials under 200 rpm shaking speed. We can conclude from Fig. 5 that the adsorption process of phenol-based on the eco-friendly biosorbent is inversely proportional to the phenol concentrations.

By studying the effect of phenol concentration on the degree of absorption efficiency, the results showed that the maximum removal of phenol using unmodified DPF and modified Si-DPF nanomaterials was 76 and 84 ppm of phenol from aqueous solution held 100 ppm of phenol concentration. Thus, the process efficiency alters from 33 to 76 % for DPF and 49 to 84 % for SI-DPF nanomaterials. The high adsorption capability of the biosorbent nanomaterials at a low initial concentration of phenol may be attributed to the competence of the phenol molecules to the numerous active sites that exist on the biosorbent surfaces on DPFNPs and Si-DPF nanomaterials.

Conversely, at a higher concentration of the initial phenol molecules, the adsorption efficiency of the biosorbent nanomaterials decreases. This can be referred to as the monolayer-adsorption process of phenol molecules on the biosorbent surface. The formed monolayer reduces the adsorption process

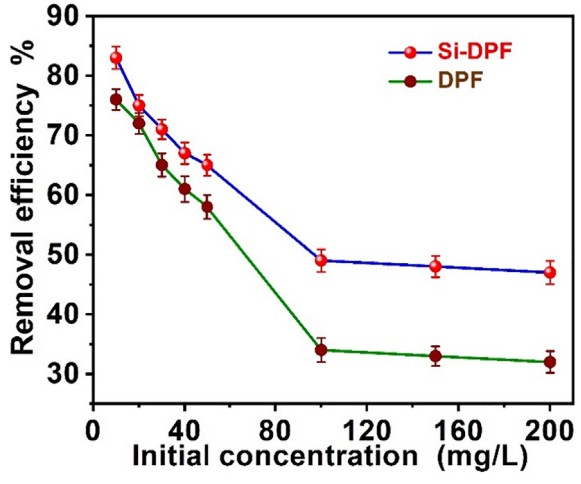

Fig. 5 Influence of the initial phenol content on the DPF (bottom) and Si-DPF (top) nanomaterials surfaces, Time of reaction = 24 h, room temperature, shaking rate of 200 rpm, and neutral pH medium.

efficiency and therefore quenches the phenol removal proficiency due to the time demanded to reach the adsorption equilibrium point on DPF, and Si-DPF nanomaterials surfaces were predictable to be retentive at a higher phenol ions content than at lower initial phenol ions content (Younis et al., 2020). We can conclude that the optimum initial phenol concentration in the proposed research was 100 ppm at the dose of biosorbent is 100 mg. This presented concept was noticed in the phenol removal process on the lemena geba (Younis and Nafea 2015).

3.5. pH influences

Herein, we investigated the influence of the pH on the adsorption efficiency of phenol removal based on the biosorbent nanomaterials. The optimum conditions of the experiment series were chosen to be the concentration of phenol molecules at 100 ppm, the concentration of biosorbent is 100 ppm, at room temperature, time = 24 h, and under shaking speed of 200 rpm. The phenol removal process was affected by presenting amino groups to the DPF biosorbent surface. The zeta potential values were utilized as an essential tool to follow the considerable changes in the adsorption process. The results were collected for both unmodified and modified DPF nanomaterials at various pH aqueous solutions. In a neutral medium, at pH 7, unmodified DPF shows a –32 mV zeta potential value. This value was turned into + 15 mv after modifying the outer surface of DPF by APTS molecules. The successful labeling will increase the amino groups on the surface of the biosorbent that turning the potential into a positive value. In addition, in acidic medium pH ~ 3, the presence of access hydrogen proton will increase the positive potential values of unmodified and modified biosorbent to + 22 and + 28 mV, respectively.

The increment of the positive potential of biosorbent can be referred to as the protonated active groups on their surfaces at this definite pH. This leads to the multiple values of the positive potential of the modified nanomaterials. The protonated amino groups attract the phenolate ions that bear negative charges. Thus, the adsorption process of the modified nanomaterials increases efficiently. Furthermore, the pK_a value of the phenol molecules is 9.95. This value stabilizes the phenol molecules to some limit, resulting in quenching the adsorption process because of the net repulsion forces between biosorbent and phenoxide ions. Conversely, under acidic conditions, the existence of a positive charged zeta potential of DPF or Si-DPF nanomaterials enhances the static attraction forces between the biosorbent surface and the phenolate ions. This causes an increment in the adsorption efficiency. The obtained results are acceptable to some earlier literature (Mirian and Nezamzadeh-Ejhieh 2016). Finally, at pH ~ 10, unmodified DPF and modified Si-DPF nanomaterials reach −38 and −28 mV, respectively, as exhibited in Fig. 6. All the functional groups of unmodified DPF and Si-DPF nanomaterials were deprotonated and became negatively charged, so interrupting the adsorption process efficacy. Thus, the adsorption efficiency becomes poor due to the increment of the repulsion forces between phenol molecules and the biosorbent, which slows down the adsorption process and deactivates the surfaces of the biosorbent.

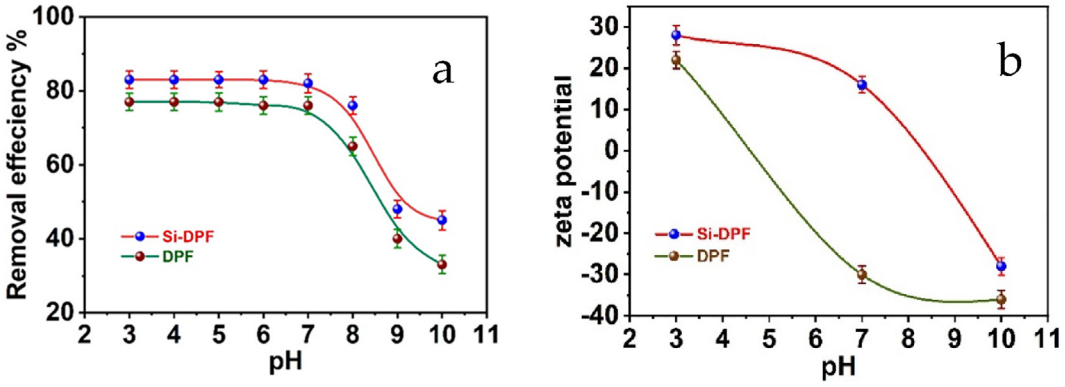

Fig. 6 (a) pH influences the adsorption efficiency; and (b) pH influences zeta potentials values of DPF (bottom) and Si-DPF (top) nanomaterials.

3.6. Adsorption isotherms studies

The adsorption isotherm studies the process that includes the equilibrium state between the adsorbent molecules in the solid phase and the dissolved adsorbate molecules in a liquid state. The adsorbate molecules are statically bounded to the surface of the nanomaterials. The adsorption process was studied at a constant temperature (Sheela et al., 2012). The maximum adsorption capacity of the phenol molecules to the surface of the solid biosorbent particles was estimated based on the adsorption isotherm models. To examine the adsorption mechanism of the phenol molecules to the surface of the unmodified or modified solid molecules, we utilized two models, including Langmuir and Freundlich isotherms. Fig. 7 exhibits the factors that affect the isotherm model of the adsorbate in the liquid phase that is bound to the surface of the solid adsorbent molecules. The Langmuir equation shows the adsorption process depending on the monolayer of adsorbate molecules to the surface of the solid phase of the adsorbent (Jain et al., 2009). Therefore, when the system reaches the equilibrium state, the outer surface of the solid adsorbent is saturated with a monolayer adsorbate molecule. And all the active sites on the solid biosorbent are flooded, and the adsorption process stops.

The results of the Langmuir isotherm model confirm the adsorption process with regression information of 0.9848 and 0.9971 for DPF and modified Si-DPF nanomaterials, respectively. On the other hand, Q_{max} value for monolayer capacity of Si-DPF greater than DPF exposed the enhancement of the total active sites of Si-DPF nanomaterials are accessible for the adsorption phenomenon. In the case of a multilayer adsorption isotherm (Joseph et al., 2011), Freundlich experimental model is presented and employed for a heterogeneous solid phase adsorbent surface (Wang et al., 2007). Freundlich constants KF exhibit more excellent adsorption attendance, showing outstanding capacity and intensity. Table 1 gives KF and n values estimated depending on the plot's intercept and slope (Fig. 7). The R^2 values are 0.96055 and 0.97193 for DPF and Si-DPF nanomaterials, respectively. The R^2 quantities of Langmuir isotherm are estimated to show lesser values. The exhibited n value was calculated to give a value of more than one, this indicates that the adsorption process provided by the phenol molecules on the active site of the adsorbent surface-based chemisorption mechanism. The results of the study show that it agrees with the Langmuir isotherm which

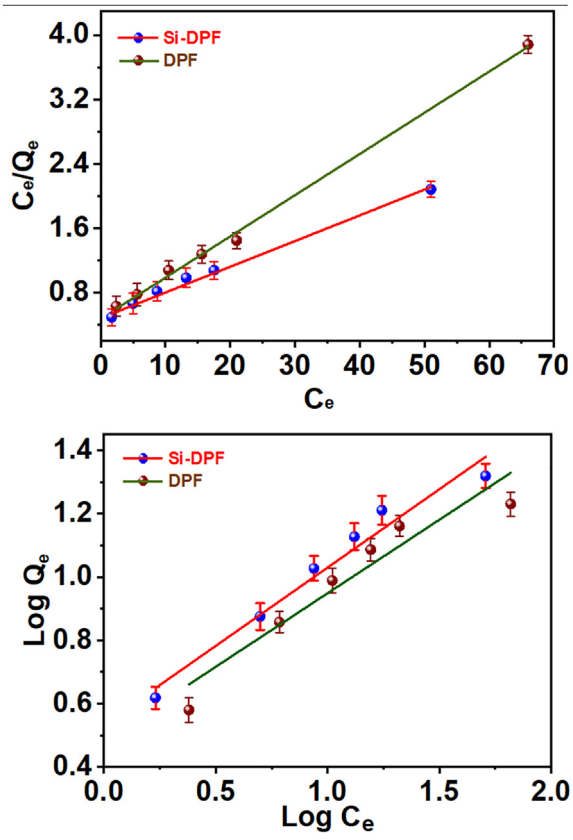

Fig. 7 Langmuir and Freundlich models.

shows the high coordination of the Langmuir monolayer model and phenol adsorption by DPF. Because the Langmuir isotherm assumes a homogeneous adsorbent surface, this coordination may be due to the homogeneous distribution of adsorption sites on the adsorbent surface. Although the Langmuir monolayer adsorption model was proper to be adequate for describing the experimental data from the adsorption tests, the Freundlich model was also used to assess the adsorption process, and it was found that the Freundlich model describes phenol adsorption as well as the Langmuir model. So, the Langmuir isotherm model is more compatible with the resulting data of the adsorption process using DPF or Si-DPF nano-

Table 1 Langmuir and Freundlich parameters.

Adsorbent	Langmuir			Freundlich		
	Q_{max} (mg/g)	K_L (L/mg)	R^2	n	K_F	R^2
SI-DPF	31.3479	0.06604	0.9971	2.02089	3.4261	0.97193
DPF	19.5695	0.10758	0.9848	2.15308	3.0483	0.96055

materials surfaces. Q_{max} at room temperature as calculated based on the Langmuir equation were 31.35 and 19.57 mg/g. the obtained data confirm that DPF and Si-DPF are effective biosorbents for phenol removal.

3.7. Kinetics of the adsorption of phenol onto DPF and Si-DPF.

The mechanism and the rate determine step involving the adsorption attendance of the phenolate ions to the active sites on the solid DPF and Si-DPF nanomaterials adsorbents were studied. The shaking time influences the adsorption process, and the results are shown in Fig. 8. Additionally, it is notably displayed that the phenolate ions adsorption of molecules on the surface of DPF and Si-DPF nanomaterials is considerably enhanced. Then equilibrium is established after 24 h. Fig. 8 is presented kinetically based on three models pseudo-first-order, pseudo-second-order, and intra-particle diffusion. The adsorption rate phenomenon between the phenolate ions and the solid adsorbent was estimated depending on the isotherm model. Besides, the proposed mechanism of the DPF adsorption process was explored. The results of the equilibrium uptake time of ~ 24 h of the current study agree with previous studies (Banat et al., 2004) while lower than recent works (Hairuddin et al., 2019; Aremu et al., 2020).

3.7.1. Pseudo-first order

The pseudo-first-order equation states that (Smičiklas et al., 2008):

$$\text{Log}\ (q_e – q_t) = \log q_e – k_1 t.$$

Where.

q_e (mgg^{-1}) = amount of adsorbate/solid nanomaterials at equilibrium.

q_t (mgg^{-1}) = adsorption capacity at time t (min).

The rate constant of pseudo-first-order was stated as $k_1(min^{-1})$.

Fig. 9 introduces the relations of log ($q_e – q_t$) against time (t).

The slope and intercept propose the rate constants (K_1) and the theoretical adsorption capacities (q_e) respectively, (see Table 2).

3.7.2. Pseudo-second-order rate model

The pseudo second order equation is shown as following:

$$t/q_t = 1/k_2 q_e^2 + t/q_e.$$

Where q_e and q_t are giving the rate constant of pseudo-second-order k_2 (g $mg^{-1}min^{-1}$) that can be determined from the plot of t/q versus time t of the adsorption process. Fig. 10 gives the plots of t/q_t versus time (t) that produce linear relation expressed by several parameters including the pseudo-second-order rate constants (k_2) and the maximum adsorption capacities (q_e) and (q_{theo}), respectively, see Table 2.

Taking into consideration the values of R^2 coefficients, adsorption capacity (q_e), and theoretical capacity (q_{theo}) of the pseudo-first and pseudo-second-order models. R^2 values of pseudo-second-order are greater than that of pseudo-first-order. Besides, the q_e and q_{theo} values deal with the results obtained from the adsorption experiments. This reveals that the adsorption process based on DPF or Si-DPF nanomaterials is a second-order kinetic model.

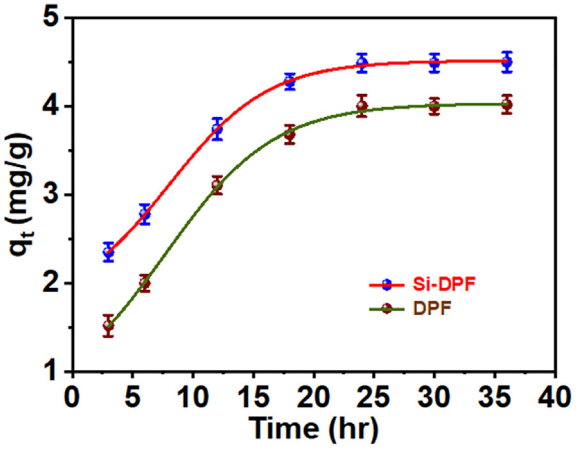

Fig. 8 Influence of the adsorption efficiency using DPF (bottom) and Si-DPF (top) nanomaterials.

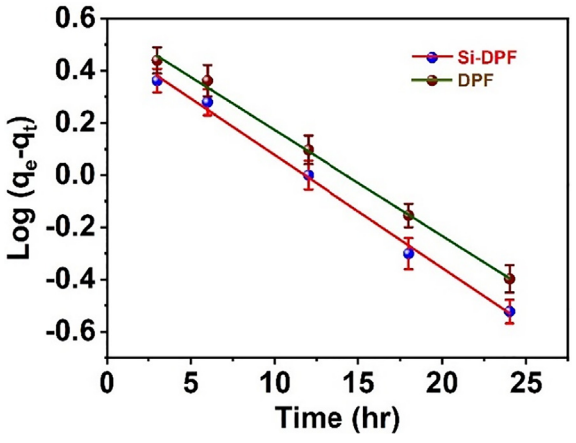

Fig. 9 . The pseudo-first-order kinetic model for the phenolate ions adsorption on DPF (top) and Si-DPF (bottom) solid nanomaterials at a time (T).

Table 2 Pseudo-first order and pseudo-second-order based on DPF and SI-DPF.

Nanomaterials	*Exp. Value/q_e ($mg.g^{-1}$)*	First-order			Second-order		
		K_1	q_e	R^2	K_2	q_e	R^2
Si-DPF	82.52	0.043	3.784	0.9843	0.0429	5.206	0.996
DPF	73.85	0.040	3.236	0.9877	0.0214	4.984	0.998

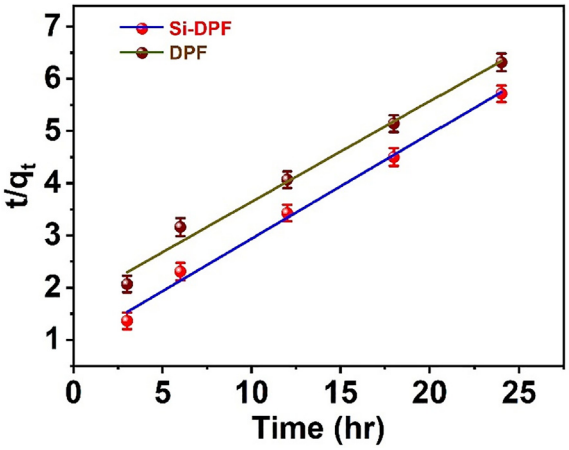

Fig. 10 Pseudo-second order model DPF (top) and Si-DPF (bottom).

3.8. Adsorption capacities comparison

The maximum adsorption capacities of DPF for phenol adsorption in comparison with different biomaterials which were studied earlier are exhibited in Table 3. The phenol adsorption capacity exhibited by the prepared SI-DPF is greater than that of most biomaterials listed in Table 3 aside from the values achieved by modified or unmodified data pits activated carbon.

Table 3 Adsorption capacities comparison.

Adsorbent	qe (mg/g)	Reference
Raw date pits	2.852	[Banat et al., 2004]
Magnetic palm kernel biochar	10.84	[Hairuddin et al., 2019]
Activated date pits	46.076	[Merzougui and Addoun 2008]
Date pits activated carbon	169.49	[Alhamed 2009]
Date stone activated carbon	111.5	[Belhachemi et al., 2009]
Modified date pits activated carbon	161.8	[Okasha and Ibrahim 2010]
Silver nanoparticle modified Palm Kernel Shell Ac	28.33	[Okasha and Ibrahim 2010]
Dried Date palm fibers (DPF)	19.5695	Present work
Si-DPF nanomaterials (Si-DPF)	31.3479	Present work

4. Conclusion

The outcome of the proposed work concludes that the DPF and Si-DPF nanomaterials exhibit significant adsorption features with phenol molecules as a severe pollutant in wastewater. It was also acquired that Si-DPF nanomaterials were additional active sorbent than dried DPF nanomaterials for the phenol removal efficacy from water. Removing phenol utilizing dried DPF nanomaterials and Si-DPF nanomaterials depends on adsorbent concentration, phenol molecule content, and contact time.

The higher adsorption efficiencies for DPF and Si-DPF respectively were 76 and 85 ppm from an aqueous solution containing 100 ppm of phenol concentration, under optimum conditions (pH: 7.00, adsorbent dose: 2.00 g/L, initial concentration of phenol: 100 ppm and contact time: 24 h).

Langmuir and Freundlich's isotherms were analyzed to detect the adsorption of the phenol molecule to the sorbent surface of the developed materials, including dried DPF and Si-DPF nanomaterials. The results of the Langmuir isotherm model confirm the adsorption process with regression information of 0.9848 and 0.9971 for DPF and modified Si-DPF nanomaterials, respectively. Thus, the Langmuir isotherm model was, largely, deals meaningfully with the practical results.

Three different adsorption kinetic models involving pseudo-first-order, pseudo-second-order, and intra-particle diffusion elucidate the adsorption kinetics results. The results display the adsorption mechanism onto the surfaces of dried DPF nanomaterials and Si-DPF, palm fibers nanomaterials, which are of the pseudo-second-order kinetic model.

As a result, this scientific research, concluded that dried DPF nanomaterials and modified Si-DPF can be utilized as a new technique for removing phenol compound by adsorption mechanism.

Acknowledgement

The authors extend their appreciation to the Deputyship for Research& Innovation, Ministry of Education and, Saudi Arabia for funding this research work through the project number (QU-IF-1-1-4). The authors also thank to the technical support of Qassim University.

Funding

The research receives the specific grant from the Deputyship for Research& Innovation, Ministry of Education and, Saudi Arabia for funding (QU-IF-1-1-4).

References

Ahmad, T. et al, 2012. The use of date palm as a potential adsorbent for wastewater treatment: a review. Environ. Sci. Pollut. Res. 19, 1464–1484.

Ahmad, M.A., Alrozi, R., 2011. Removal of malachite green dye from aqueous solution using rambutan peel-based activated carbon:

Equilibrium, kinetic and thermodynamic studies. Chem. Eng. J. 171 (2), 510–516.
Ali, R., Saleh, S.M., Elshaarawy, R.F., 2016. Turn-on pH nano-fluorosensor based on imidazolium salicylaldehyde ionic liquid-labeled silica nanoparticles. RSC adv. 6 (90), 86965–86975.
Al-Oqla, F.M. et al, 2014. Processing and properties of date palm fibers and its composites. Biomass bioenergy. Springer, Cham, pp. 1–25.
Alotaibi, M.D. et al, 2019. Characterization of natural fiber obtained from different parts of date palm tree (Phoenix dactylifera L.). Int. J. Biol. Macromol. 135, 69–76.
Alshabanat, M., Al-Mufarij, R.S., Al-Senani, G.M., 2016. Study on adsorption of malachite green by date palm fiber. Orient. J. Chem. 32 (6), 3139.
Alshabanat, M., Alsenani, G., Almufarij, R., 2013. Removal of crystal violet dye from aqueous solutions onto date palm fiber by adsorption technique. J. Chem. 2013.
Aremu, M.O. et al, 2020. Improved phenol sequestration from aqueous solution using silver nanoparticle modified Palm Kernel Shell Activated Carbon. Heliyon 6, (7) e04492.
Azari, A. et al, 2015. Performance evaluation of magnetized multiwall carbon nanotubes by iron oxide nanoparticles in removing fluoride from aqueous solution. Journal of J. Maz. Univ. Med. Sci. 25 (124), 128–142.
Azari, A. et al, 2021. The superior adsorption capacity of 2, 4-Dinitrophenol under ultrasound-assisted magnetic adsorption system: Modeling and process optimization by central composite design. Journal of Hazard. Mater. 418, 126348.
Badi, M.Y. et al, 2019. Degradation of dimethyl phthalate using persulfate activated by UV and ferrous ions: optimizing operational parameters mechanism and pathway. J. Environ. Health Sci. Eng. 17 (2), 685–700.
Banat, F., Al-Asheh, S., Al-Makhadmeh, L., 2004. Utilization of raw and activated date pits for the removal of phenol from aqueous solutions. Chemical Engineering & Technology: Industrial Chemistry-Plant Equipment-Process Engineering-Biotechnology 27 (1), 80–86.
Berizi, Z. et al, 2016. The study of non-linear kinetics and adsorption isotherm models for Acid Red 18 from aqueous solutions by magnetite nanoparticles and magnetite nanoparticles modified by sodium alginate. Water Sci. Technol. 74 (5), 1235–1242.
Dahiya, D., Nigam, P.S., 2020. Waste management by biological approach employing natural substrates and microbial agents for the remediation of dyes' wastewater. App. Sci. 10 (8), 2958.
Dehmani, Y., 2020. Removal of phenol from aqueous solution by adsorption onto hematite (α-Fe2O3): mechanism exploration from both experimental and theoretical studies. Arab. J. Chem. 13 (5), 5474–5486.
Du, Q. et al, 2014. Highly enhanced adsorption of congo red onto graphene oxide/chitosan fibers by wet-chemical etching off silica nanoparticles. Chem. Eng. J. 245, 99–106.
Elbadry, E.A., 2014. Agro-residues: surface treatment and characterization of date palm tree fiber as composite reinforcement. J. Compos. 2014.
Eryılmaz, C., Genc, A., 2021. Review of treatment technologies for the removal of phenol from wastewaters. J. Water Chem. Technol. 43 (2), 145–154.
Esrafili, A. et al, 2016. Removal of diethyl phthalate from aqueous solution using persulfate-based (UV/Na2S2O8/Fe2+) advanced oxidation process. J. Maz. Univ. Med. Sci. 25 (132), 122–135.
Ghori, W. et al, 2018. A review on date palm (phoenix dactylifera) fibers and its polymer composites 368, 012009.
Gül, Ü.D., Ilhan, S., İşçen, C.F., 2019. Optimization of Biosorption Conditions for Surfactant Induced Decolorization by Anaerobic Sludge Granules. Tenside Surfactants Detergents 56 (3), 188–196.
Guo, H. et al, 2018. Construction of direct Z-scheme AgI/Bi2Sn2O7 nanojunction system with enhanced photocatalytic activity: accelerated interfacial charge transfer induced efficient Cr (VI) reduction, tetracycline degradation and Escherichia coli inactivation. ACS Sustain. Chem. Eng. 6 (6), 8003–8018.
Guo, Y. et al, 2022. Contemporary antibiofouling modifications of reverse osmosis membranes: State-of-the-art insights on mechanisms and strategies. Chem. Eng. J. 429, 132400.
Hairuddin, M.N. et al, 2019. Magnetic palm kernel biochar potential route for phenol removal from wastewater. Environ. Sci. Pollut. Res. 26 (34), 35183–35197.
Hassan, M.S., Salih, W.M., 2016. Mechanical Performance of CO_2 and autoclave cured date palm fiber reinforced eco-mortar composites. J. Eng. Technol. 34, 14.
Jain, M., Garg, V.K., Kadirvelu, K., 2009. Chromium (VI) removal from aqueous system using Helianthus annuus (sunflower) stem waste. J. Hazard. Mater. 162 (1), 365–372.
Joseph, L. et al, 2011. Adsorption of bisphenol A and 17α-ethinyl estradiol on single walled carbon nanotubes from seawater and brackish water. Desalination 281, 68–74.
Karim, A.H. et al, 2012. Amino modified mesostructured silica nanoparticles for efficient adsorption of methylene blue. J. Colloid Interface Sci. 386 (1), 307–314.
Khurshid, H., et al, 2022. A Comprehensive Insight on Adsorption of Polyaromatic Hydrocarbons, Chemical Oxygen Demand, Pharmaceuticals, and Chemical Dyes in Wastewaters Using Biowaste Carbonaceous Adsorbents. Adsorp. Sci. Technol. 2022.
Lalhruaitluanga, H. et al, 2010. Lead (II) adsorption from aqueous solutions by raw and activated charcoals of Melocanna baccifera Roxburgh (bamboo)-a comparative study. J. Hazard. Mater. 175 (1–3), 311–318.
Mader, H. et al, 2008. Fluorescent silica nanoparticles. Ann. N. Y. Acad. Sci. 1130 (1), 218–223.
Mani, A., Hameed, S.A.S., 2019. Improved bacterial-fungal consortium as an alternative approach for enhanced decolourisation and degradation of azo dyes: a review. Nat. Environ. Pollut. Technol. 18 (1), 49–64.
Merzougui, Z, Addoun. 2008. F. Effect of oxidant treatment of date pit activated carbons application to the treatment of waters. Desalination 1(222), 394-403.
Mirian, Z.A., Nezamzadeh-Ejhieh, A., 2016. Removal of phenol content of an industrial wastewater via a heterogeneous photodegradation process using supported FeO onto nanoparticles of Iranian clinoptilolite. Desalin. Water Treat. 57 (35), 16483–16494.
Moghaddam, M.H. et al, 2019. Performance investigation of Zeolitic Imidazolate framework–8 (ZIF-8) in the removal of trichloroethylene from aqueous solutions. Microchem. J 150, 104185.
Moreno-Marenco, A.R., Giraldo, L., Moreno-Piraján, J.C., 2020. Adsorption of n-butylparaben from aqueous solution on surface of modified granular activated carbons prepared from African palm shell. Thermodynamic study of interactions. J. Environ Chem. Eng. 8, (4) 103969.
Okasha, A.Y., Ibrahim, H.G., 2010. Phenol removal from aqueous systems by sorption of using some local waste materials. Elec. J. Env. Agricult. Food Chem. 9, 796–807.
Pasalari, H. et al, 2017. Activated carbon derived from date stone as natural adsorbent for phenol removal from aqueous solution. Desalin. Water Treat. 72, 406–417.
Ragab, T.I. et al, 2021. Enhanced Optimization of Bioethanol Production from Palm Waste Using the Taguchi Method. Sustainability 13 (24), 13660.
Raghavendra, S., Lokesh, G. N., 2019. Evaluation of mechanical properties in date palm fronds polymer composites. In AIP Conference Proceedings. 2057(1), 020021. AIP Publishing LLC.
Routoula, E., Patwardhan, S.V., 2020. Degradation of anthraquinone dyes from effluents: a review focusing on enzymatic dye degradation with industrial potential. Environ. Sci. technol. 54 (2), 647–664.
Saker, M.M. et al, 2006. Monitoring of cultivar identity in tissue culture-derived date palms using RAPD and AFLP analysis. Bio. Plant. 50 (2), 198–204.

Saleem, J., Shahid, U.B., Hijab, M., Mackey, H., McKay, G., 2019. Production and applications of activated carbons as adsorbents from olive stones. Biomass Convers. Biorefin. 9 (4), 775–802.

Saleh, S.M. et al, 2010. Novel multicolor fluorescently labeled silica nanoparticles for interface fluorescence resonance energy transfer to and from labeled avidin. Anal. Bioanal. Chem. 398 (4), 1615–1623.

Saleh, S. et al, 2019. Phenol removal from aqueous solution using amino modified silica nanoparticles. Korean J. Chem. Eng. 36 (4), 529–539.

Saleh, S.M., Ali, R., Wolfbeis, O.S., 2011. New silica and polystyrene nanoparticles labeled with longwave absorbing and fluorescent chameleon dyes. Microchim. Acta 174 (3), 429–434.

Sanchez, L.M. et al, 2018. Nanocomposite materials for dyes removal. In: Handbook of Nanomaterials for Industrial Applications. Elsevier, pp. 922–951.

Sheela, T. et al, 2012. Kinetics and thermodynamics studies on the adsorption of Zn (II), Cd (II) and Hg (II) from aqueous solution using zinc oxide nanoparticles. Powder Technol. 217, 163–170.

Singh, L.P. et al, 2014. Sol-Gel processing of silica nanoparticles and their applications. Adv. Colloid Interface Sci. 214, 17–37.

Siva Kumar, N.A.D.A.V.A.L.A., Min, K., 2011. Removal of phenolic compounds from aqueous solutions by biosorption onto Acacia leucocephala bark powder: Equilibrium and kinetic studies. J. Chil. Chem. Soc. 56 (1), 539–545.

Smičiklas, I. et al, 2008. Factors influencing the removal of divalent cations by hydroxyapatite. J. Hazard. Mater. 152 (2), 876–884.

Stöber, W., Fink, A., Bohn, E., 1968. Controlled growth of monodisperse silica spheres in the micron size range. J. Colloid Interface Sci. 26 (1), 62–69.

Sun, B. et al, 2015. Reduction of acute inflammatory effects of fumed silica nanoparticles in the lung by adjusting silanol display through calcination and metal doping. ACS Nano 9 (9), 9357–9372.

Thommes, M. et al, 2015. Physisorption of gases, with special reference to the evaluation of surface area and pore size distribution (IUPAC Technical Report). Pure Appl. Chem. 87 (9–10), 1051–1069.

Wang, X. et al, 2007. Sorption of aromatic organic contaminants by biopolymers: Effects of pH, copper (II) complexation, and cellulose coating. Environ. Sci. Technol. 41 (1), 185–191.

Wang, S. et al, 2015. Adsorption of Pb^{2+} on amino-functionalized core–shell magnetic mesoporous SBA-15 silica composite. Chem. Eng. J. 262, 897–903.

Younis, A.M. et al, 2016. Low cost biosorbent (Lemna gibba L.) for the removal of phenol from aqueous media. J. mediterr. ecol. 14, 55–62.

Younis, A.M., Nafea, E.M., 2015. Heavy metals and nutritional composition of some naturally growing aquatic macrophytes of Northern Egyptian Lakes. J. biodivers. environ. sci. 6 (3), 16–23.

Younis, A.M., Elkady, E.M., Saleh, S.M., 2020. Novel eco-friendly amino-modified nanoparticles for phenol removal from aqueous solution. Environ. Sci. Pollut. Res. 27 (24), 30694–30705.

Yousefzadeh, S. et al, 2017. A comparative study of anaerobic fixed film baffled reactor and up-flow anaerobic fixed film fixed bed reactor for biological removal of diethyl phthalate from wastewater: a performance, kinetic, biogas, and metabolic pathway study. Biotechnol. Biofuels 10 (1), 1–15.

Youssif, M.I. et al, 2018a. Sol-Gel Tailored Synthesized Nanosilica for Enhanced Oil Recovery in Water-Wet and Oil-Wet Benthemier Sandstone. Energy Fuels 32 (12), 12373–12382.

Youssif, M.I. et al, 2018b. Silica nanofluid flooding for enhanced oil recovery in sandstone rocks. Egypt. J. Pet. 27 (1), 105–110.